INDONESIAN JOURNAL ON GEOSCIENCE
Geological Agency
Ministry of Energy and Mineral Resources

Journal homepage: https://ijog.geologi.esdm.go.id
ISSN 2355-9314, e-ISSN 2355-9306

Analysis of Lithological Aspects and Their Influence on Slope Stability of the Failed Riverbank in Ajil, Hulu Terengganu, Malaysia

Sofea Razali[2], Muhd Nur Ismail Abdul Rahman[1,2*], Siti Syaza Aiman Seh Wali[2], Dony Adriansyah Nazarudin[2], Muhamad Zaki Zulkifli[2], Ahmad Nor Zaimie Roslan[3], and Effi Helmy Ariffin[4]

[1]Aqua Heritage Research Interest Group, Faculty of Science and Marine Environment, Universiti Malaysia Terengganu 2023 Kuala Nerus, Terengganu, Malaysia
[2]ROCK Research Interest Group Faculty of Science and Marine Environment, Universiti Malaysia Terengganu 2023 Kuala Nerus, Terengganu, Malaysia
[3]Mineral and Geoscience Department Malaysia PT3102K, Jalan Sultan Sulaiman, 20200 Kuala Terengganu, Terengganu, Malaysia
[4]Institute of Oceanography and Environment, Universiti Malaysia Terengganu, Kuala Nerus, Terengganu 21030, Malaysia

*Corresponding Author: nur.ismail@umt.edu.my
Manuscript received: September, 15, 2024; revised: July, 28, 2025;
approved: September, 24, 2025; available online: October, 30, 2025

Abstract - Riverbank erosion has become a serious problem in Hulu Terengganu River recently. In some locations, the failed riverbank is particularly hazardous, especially near recreational and plantation areas. Therefore, this study aims to assess the lithological characteristics controlling the failed riverbank in Ajil, Hulu Terengganu, Malaysia. Two localities were chosen based on the hazardous conditions and severity of erosion along the riverbanks. Both riverbanks were vertically logged to differentiate lithological units. Field observations identified four lithological horizons, designated as Litho A-D, based on in-situ characteristics (*i.e.* structure, plant roots, grain size). Samples were taken from selected horizons for Particle Size Analysis (PSA) and Atterberg limit testing. The results of the investigation from PSA indicate that the samples from localities L1S1, L2S1, L1S2, and L2S2 exhibit positive skewness, with fine sediment sizes identified as silt-clay for L1S1 and L1S2, and sand-silt for L2S1 and L2S2. Conversely, samples L1S3 and L2S3 demonstrate a trend of negative skewness, indicating coarse sediment sizes. The results indicate that the sand-silt composition suggests a decrease in water flow energy from high to low. The coefficient of uniformity (Cu) in this study ranged between 3.6 to 9.81, and the coefficient of curvature (Cc) ranged from 0.63 to 1.66. The Cc values for L1S3 and L2S3 are below 1.0 indicating well-graded soil, while the Cc values for other samples are above 1.0 indicating poorly graded soil.

Keywords: Hulu Terengganu, lithological unit, particle size analysis (PSA), Atterberg limits, coefficient of uniformity (Cu), coefficient of curvature (Cc)

How to cite this article:
Razali, S., Rahman, M.N.I.A., Wali, S.S.A.S., Nazarudin, D.A., Zulkifli, M.Z., Roslan, A.N.Z., and Ariffin, E.H., 2025. Analysis of Lithological Aspects and Their Influence on Slope Stability of the Failed Riverbank in Ajil, Hulu Terengganu, Malaysia. *Indonesian Journal on Geoscience*, 12 (3), p.367-382. DOI: 10.17014/ijog.12.3.367-382

Introduction

Background

Several rivers in Malaysia are prone to hazards due to factors such as deforestation, flooding, and sand mining. These factors can lead to riverbank failure, where the banks experience hydraulic erosion (Julian and Tores, 2006; Huang *et al*., 2021; Duan *et al*., 2024) and geotechnical instability (Islam, 2008; Taha *et al*., 2022; Razali *et al.*, 2023).

Hydraulic instability can be caused by erosion beneath a somewhat stable bank, unpredictable floods, sediment debris, removal of bank vegetation, loosening of coarse sediment (gravel) by wave action, secondary currents, and other factors (Darby and Thorne, 1996; Ahmed, 2001; Duró *et al*., 2020; Hao *et al*., 2023). Toriman and Che' Lah (2007) explain that erosion, transportation, and sedimentation in rivers are natural processes that help shape a river balance. River balance is influenced by time factors according to their respective stages. The rate of river erosion occurs faster in larger retivers compared to smaller river channels. According to Lemnitzer *et al*. (2023), the mechanism of riverbank erosion produces extensive undercutting effects at the bottom of steep banks, resulting in landslides when the water level is high. Riverbank erosion can occur due to a single factor or a combination of several factors simultaneously, such as the loss of soil particles in the bank structure by river flow and soil slippage (Toriman and Che'Lah, 2007). Slippage is caused by an increase in the slope of the bank due to natural erosion or engineering works. Additionally, erosion beneath the riverbank caused by turbulent currents, as well as lateral erosion, can lead to riverbank failure.

In Malaysia, the detailed causes of riverbank erosion are still not well understood, especially when it comes to the morphology of the river, the strength of the soil, and the overall stability of the banks (Toriman, 2005; Chassiot *et al*., 2020; Razali *et al*., 2023). Most local studies focus on general factors such as rainfall, the amount of sediment carried by the river, and water flow (Gasim *et al*., 2005a; Lemnitzer *et al*., 2023). In other parts of the world, however, riverbank erosion has been widely studied, especially near river mouths and deltas where erosion problems are most serious (Toriman, 1997; Baracos and Lew, 2003; Duan *et al*., 2024). Many of these studies are from temperate and polar regions (Chassiot *et al*., 2020), but research in tropical areas like Malaysia is still limited. This gap is important, because the type of soil and rock plays a big role in how riverbanks behave. In Malaysia, riverbanks are mostly made of sand, silt, clay, and ferric oxide, which are very different from the loess, glacial till, or frozen soils found in colder regions. These differences show why detailed soil and rock studies are needed in tropical rivers to better understand and prevent riverbank failures.

This study will primarily focus on the Berang River, which serves as the main water drainage system in the Ajil area, delineated by latitudes N 5°5' and N 4°50', and longitudes E 102°50' and E 103°10' (Figures 1a and b). The river stretches approximately 30 km from The Belukar Bukit waterfall to the main Terengganu-Jenagor River Junction. It plays a crucial role in the hydrological cycle of the Ajil area. Given that the surrounding area is inhabited by residents and contains oil palm plantations, in addition to being a popular recreational spot, the river also functions as an agricultural drainage channel. However, the river presence also contributes to cliff erosion, and poses a risk of flooding during heavy rains. This study will focus specifically on two localities, labeled as Locality 1 and Locality 2, chosen based on the hazardous conditions and severity of erosion along the riverbanks. These areas were selected due to severe erosion observed following continuous heavy rainfall and landslides in February 2022. As a result of this incident, small buildings, pedestrian walkways, access roads, and trees were washed away. Given these circumstances, the study aims to examine the lithological aspects contributing to riverbank failure.

General Geology

Geology of the Hulu Terengganu area comprises metasedimentary rocks, igneous rocks, and alluvial plains (Sharoum *et al*., 2015; Rahman *et al*., 2023). Geological information from the Ajil and Kuala Berang areas indicates that these regions consist of Carboniferous-aged sedimentary rocks (approximately 350 million years old) and intrusive igneous rocks such as granite and gabbro (approximately 259 - 250 million years old). The metamorphosed sedimentary rocks in the Hulu Terengganu area constitute the oldest rock sequences extensively exposed in the southwestern part of the studied area. These rock fragments

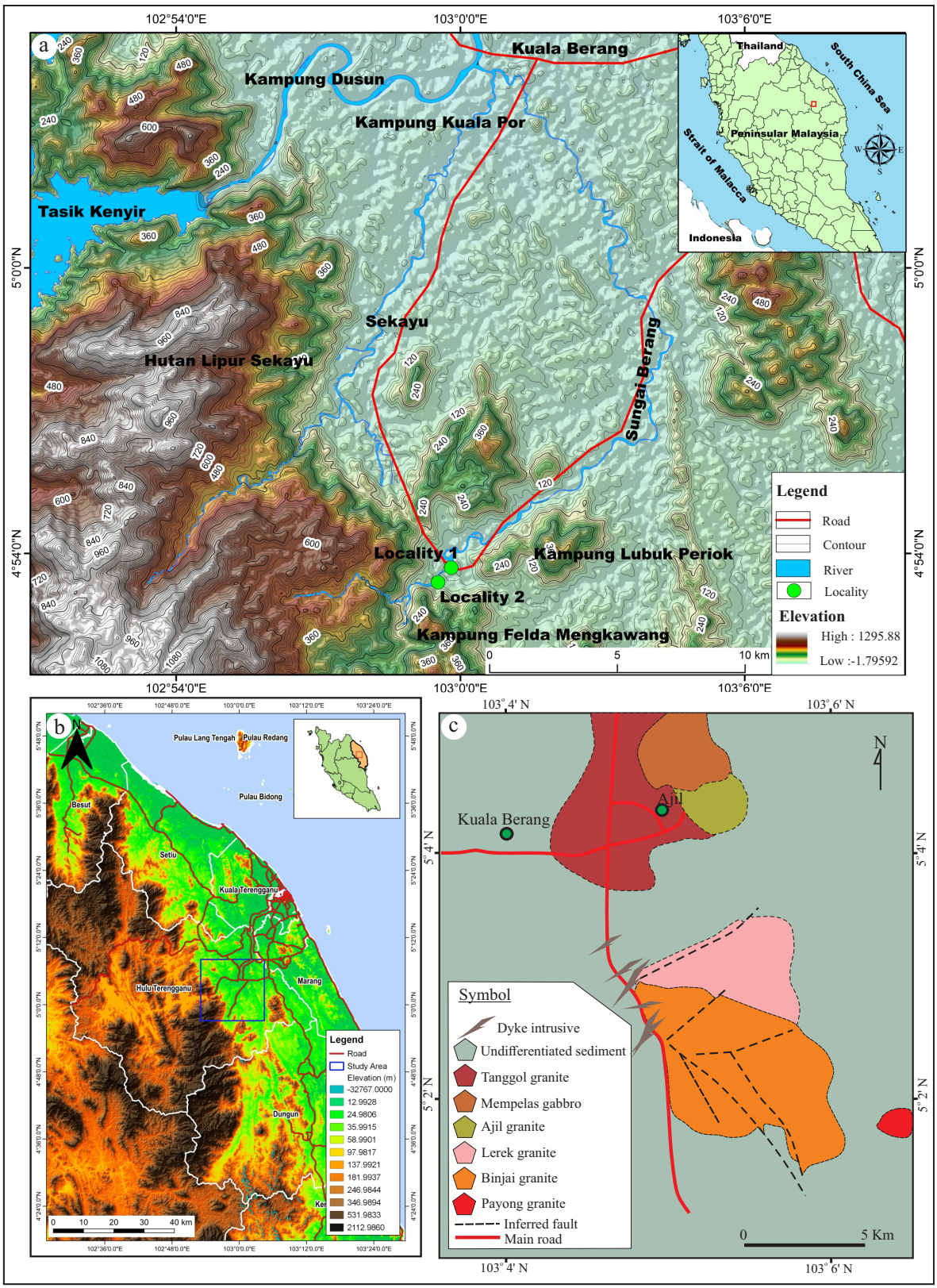

Figure 1. a) Base map showing the drainage system and also the topography of the Ajil area. b) Map of Peninsular Malaysia showing the location of the studied area in a blue box. c) Geological map of the Ajil area consisting mostly of granite rocks (modified from Badruldin *et al.,* 2017).

are widely exposed as rock blocks to gravel-sized grains in the Belukar Bukit waterfall area in Ajil. Fragments of these sedimentary rocks are also found within the Berang River channel. While granite rocks dominate in the east−west area of Ajil. These rocks are also exposed in the waterfall area, and also form hills in several places in the Ajil area. This igneous rock is included in the Tanggol granite igneous rock that connects the Kapal granite on the high hilly strip in the Lake Kenyir and its surrounding area. The granite from Ajil area according to Badruldin *et al*. (2017) comprised predominantly of Jerangau Forest Pluton (Figure 1c). The pluton is further divided into Lerek, Binjai, and Payong granites. Lerek and Binjai granites are characterized by pinkish colour, medium- to coarse-grained phaneritic texture. In addition, numerous mafic dykes were intruded and exposed in the western part of Lerek and Binjai granites along 10 km distance from KM 390 to KM 400 of East Coast Expressway.

Limited study has been conducted on the Quaternary geology, with most of the information derived from the authors' observations and analyses prior to completing the research. The alluvial plain exposed in Ajil can be classified into recent alluvium and old alluvium. Recent alluvium is prominently visible near lowland areas, especially along the river, and partially covers the sandbar regions. This recent alluvium predominantly comprises various unsorted grains, with a dominant clay-silt composition. In contrast, old alluvium is primarily distributed along the riverbank sections. The alternating horizontal sedimentary sequences exhibit distinct lithological evidence. They are slightly compacted, with a variety of grain sizes ranging from clay to gravel, forming the natural structure of the riverbank. Gravel displays imbrication and is supported by unsorted coarse to fine sand. Additionally, signs of root decay and oxidation processes are evident on the sedimentary bed. The old alluvium is older than the recent alluvium, as indicated by the preservation of its sedimentary layers. In Ajil, a significant portion of the old alluvium undergoes pedogenesis on a large scale due to its interaction with water.

Methods and Materials

Sedimentological Methods

Two riverbanks were vertically logged to differentiate the lithological units. These units were visually identified from the dominant lithology observed in the outcrop. The logged profile was used to assess the connectivity of the lithological units between these riverbanks. Furthermore, the interpretation of the observed riverbanks and recent features will provide additional information about the condition of the riverbank after the failure. The thickness of each bed was measured, and samples were taken from each lithology. The samples were then processed in the laboratory for further analysis.

Particle Size Analysis

Particle size determination analysis is a laboratory procedure aimed at determining the proportion of soil particles of varying sizes in a given sample. This analysis comprises two methods: wet and dry. A 250-gram sample will be weighed and then subjected to the dry sieve technique. The specimen will undergo dehydration in an oven set at 100^{0} C. The process of dry sieving will involve the use of sieves with specific dimensions: 4.00 mm, 2.00 mm, 1.00 mm, 0.710 mm, 0.500 mm, 0.355 mm, 0.250 mm, 0.125 mm, 0.063 mm, and <0.063 mm. The mass of the sample for each sieve size will be measured and documented. The specimen will undergo the sieving process using a sieve with a pore size of 63 micrometres.

The sieve findings with diameters smaller than 63 micrometres will be used for wet analysis, utilizing an Anton Paar apparatus for particle size analysis. Samples containing more than 10 % fine sediment will be analyzed using the laser scattering method. The PSA device utilizes laser scattering technology, directing the laser at sediment samples contained within a glass beaker. This method is suitable for determining fine particles present in soil samples. Statistical data of the sediment will be displayed on a computer using the Kalliope programme. Detecting light at specific angles offers different benefits in light

scattering measurements. "Back angle" or "back scatter" measures light scattered back toward the incident laser beam, typically at 175°, while "side scatter" refers to light scattered 90° perpendicular to the beam. "Forward scatter" detects light scattered at 15° in the same direction as the beam.

Atterberg Limit

The Atterberg limits test is performed to determine the plastic limit and liquid limit of soils with a high proportion of fine particles. Assessing the engineering features of soils affected by moisture content is of utmost importance, as it pertains to the correlation between the amount of moisture present and the engineering characteristics of the soil. The Atterberg limit test consists of three primary analyses: liquid limit, plastic limit, and shrinkage limit.

Liquid Limit, LL (ASTM D 4318)

A sample is placed within a ceramic vessel. The sample used is one that has successfully passed through a 0.425 mm sieve and has been dehydrated. A small quantity of distilled water was added to the sample to create a paste. The specimen is protected to avoid desiccation. Subsequently, the sample was introduced into a Casagrande liquid limit apparatus and leveled. The sample was partitioned using a groove tool, creating a distinct groove with no physical interaction between the two sides. The liquid limit test commenced by determining the number of impacts (N) necessary for the soil specimen to make contact with itself over a 13 mm (1/2-inch) distance. A small fraction of the sample was extracted, transferred to a porcelain dish, and weighed. The specimen was then dehydrated in a furnace for 16 hours at a temperature of 100^0 C. This method was repeated four times by incorporating distilled water. The range of blows consists of values of 10, 20, 30, 40, and 50. The goal of incrementally taking blows at ten intervals is to achieve a graph that is both smooth and easily interpretable.

Plastic Limit, PL (ASTM D 4318)

The plastic limit determination is an extension of the liquid limit test, where the soil sample obtained from the liquid limit test is reused. After being combined with water, the sample was transformed into a compact and unified substance resembling a slender thread measuring 3.2 mm in diameter (equivalent to 1/8 inch). The thread-like sample was further extended until it showed signs of fracture. Subsequently, the sample was placed into a receptacle, weighed, and the data was recorded. This technique was repeated multiple times to derive an average value. The specimen was then placed in a furnace and subjected to a drying process lasting 16 hours. Once dried, the sample was weighed again, and the weight was recorded. The plasticity index (PI) was calculated by subtracting the value of the plastic limit (PL) from the liquid limit (LL). This study allows for the plotting of LL vs. PI data on a plasticity chart to ascertain the soil type.

Result and Discussion

Field Observation and Sedimentology Characteristics

Riverbank 1

The riverbank exhibits a height of 5.2 m following a significant river overflow (Figure 2a). The logged section reveals various lithological units, which can be categorized into three main types: Litho B, Litho C, and Litho D. Litho B, approximately 1.2 m thick, is distinguished by prominent cross-bedded features. It consists of unconsolidated gravel arranged in an imbricated pattern along the upper portion of the riverbank. Samples obtained along Riverbank 1 were designated with the codes L1S1 to L1S3. Field observations indicate occasional mixing of coarse sand and silt within this area. Litho B is believed to experience high-energy processes that transport larger sediments, and produce cross-bedding features along the riverbank. Cross-bedding occurred due to the sideways and downstream movement of a channel bar, with the inclined layers being steep and slopy (Casnedi and Giulio, 1999; Saikia and Laskar, 2022). The imbrication of gravel suggests the direction of

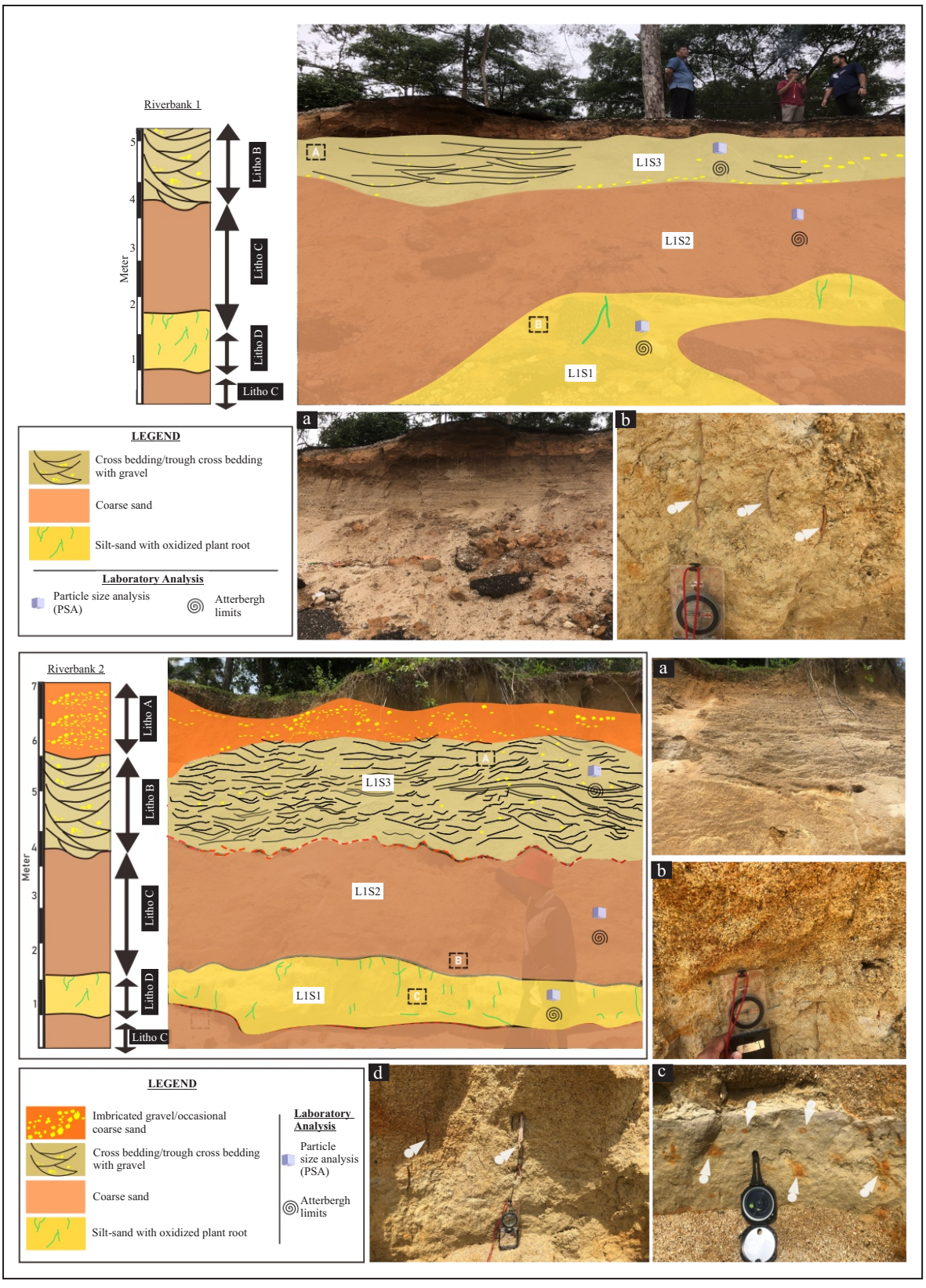

Figure 2. a) Riverbank 1 exhibits height of 5.2 m following a significant river overflow, categorize by three main types: Litho B, Litho C, and Litho D. b) Riverbank 2, recorded at 7 m above water level and categorized to four distinct lithological units: Litho A, Litho B, Litho C, and Litho D. Note that the sample identification is located on the riverbank as L1S1–L2S3.

water flow. Litho C, situated beneath Litho B and above Litho D, varies in thickness from 1 to 2 m, and displays unsorted coarse grains. This unit is interpreted as part of the river coarse sediment deposition during periods of water overflow, particularly during floods. Litho D represents the lowest section in the logged profile with 1.1 m thick, lying below Litho C. It is characterized by its thinner nature compared to the other lithological divisions, and consists mainly of sand-silt material. Litho D shows a slightly more compact bank compared to Litho B and Litho C. The sand-silt composition suggests a decrease in water flow energy from high to low. During high-energy floods and low-energy dry seasons, the water flow varies, leading to the settlement of silt. Within Litho D, numerous oxidized plant root remnants are also present, indicating past vegetation in the area. Small plants, especially marshes and bushes, can grow along the riverbank when the sand is exposed due to low river water levels. This cycle repeats each year, leaving oxidized plant material on the sand.

Riverbank 2

This riverbank was recorded at 7 m above water level, based on the logged profile (Figure 2b). The riverbank was clearly exposed when the floodwaters receded, leaving behind the characteristic features of a modern river. The bank is divided into four distinct lithological units: Litho A, Litho B, Litho C, and Litho D. Samples obtained along Riverbank 2 are designated with the codes L2S1 to L2S3. Unlike the profile of riverbank 1, Litho A is absent, possibly eroded away during a major flood event. Litho A in the logged profile is up to 1.32 m thick, consisting of gravel and coarse-grained sand. The gravel at the lower portion of Litho A is aligned in an imbricated pattern, transitioning to a mix of scattered gravel and fine-to-coarse sand grains toward the upper part. This indicates an influx of river sediment during periods of high-water flow. Imbricated gravel can serve as strong evidence of the water flow direction in a modern river channel. Litho B, also found in riverbank 2, is thicker than in riverbank 1. It measures 1.82 m in thickness, and is characterized by cross-bedding structures, such as trough cross-bedding, with granule grains partially covering the area of the riverbank. Cross-bedding forms from the lateral and downstream movement of a channel bar, with steep, sloping layers (Casnedi and Giulio, 1999). Litho B features an erosional base, indicating river scour due to swift water flow during floods. Litho C, situated below Litho B and marked by an erosional base, ranges from 1 to 3 m in thickness. Its characteristics are similar to those of riverbank 1, consisting of unsorted coarse sand. Litho D at riverbank 2 is thinner compared to its exposure at riverbank 1, and is composed of a variety of sand and silt compositions, with a notable abundance of oxidized plant roots (Figure 3).

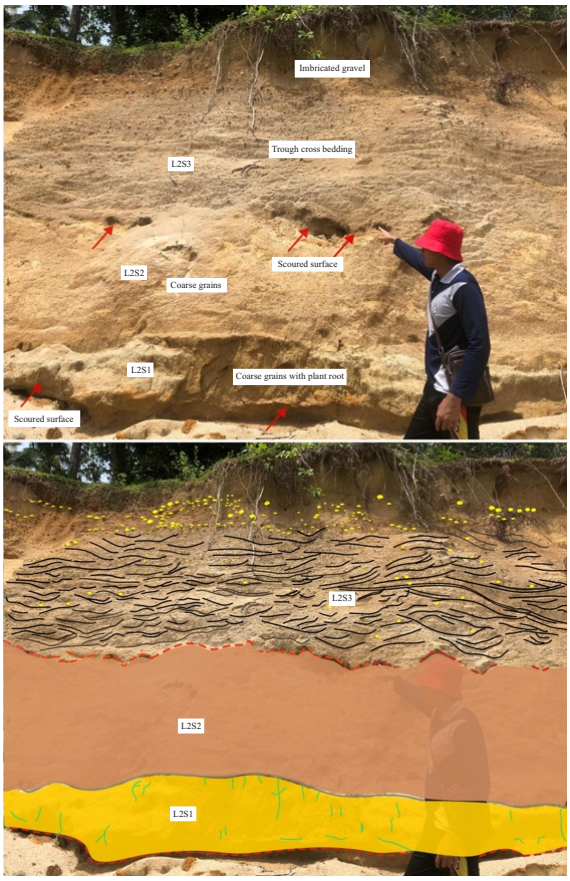

Figure 3. Lithology and erosional features on riverbank 2. There is trough, imbricated gravel, and scoured surface indication for high energy of water current. Note that the sample identification is located on the riverbank as L1S1–L2S3.

Physical Properties of Soil

Grain Size Analysis (ISO 13320)

Soil samples L1S2 and L2S2 showed a high percentage of sand (>90 %), while the other samples had higher proportions of silt and clay (Figure 4a). The obtained grain size distribution data were presented in a graph, and the results classified each sample differently, although silt dominated the percentages (Figure 4b). Each sample was also analyzed to determine the uniformity coefficient (Cu) and the coefficient of curvature (Cc) to assess the grading quality of the particles. The calculations were based on cumulative distribution values at particle sizes D10, D30, and D60, as shown in the cumulative distribution graph (Table 1). From the calculations, the uniformity coefficient (Cu) ranged from 3.6 to 9.81. The coefficient of curvature (Cc) for samples L1S1, L1S2, and L2S1 ranged from 1.05 to 1.66, while samples L1S3 and L2S3 showed values of 0.63 and 0.71. Based on this information, samples in the L1S1, L1S2, L2S1, and L2S2 areas are categorized as well-graded, while samples in the L1S3 and L2S3 areas are categorized as poorly graded (Casagrande, 1948; Das and Sobhan, 2018). According to White (2006), well-graded soil refers to soil where the spaces between the coarser and more uniform particles (silt) are filled by a range of fine-sized particles (clay), forming a denser pore structure. Poorly graded soil may indicate issues such as excessive voids, inadequate compaction, and diminished stability. The high silt content can be considered a natural defensive barrier on the riverbank, in addition to being bound by other clay minerals (particularly kaolinite). The percentage of fine particles, along with the silt content in the samples, indicates active weathering processes due to Malaysia tropical climate.

Atterberg Limits (ASTM 4318-00)

Atterberg limits refer to the moisture levels in soil at which the soil consistency changes from one state to another, marking the transition between silt and clay to other specific phases. The test involves determining the liquid limit and plastic limit of the soil. The results are then

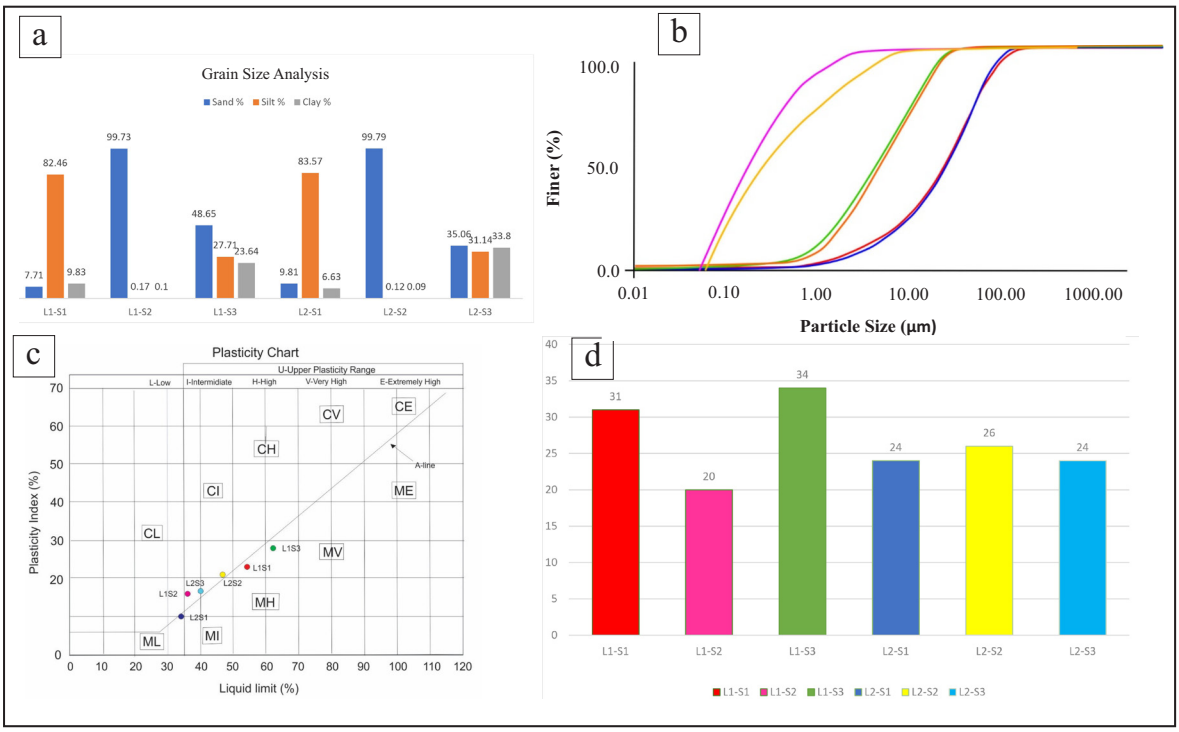

Figure 4. a) Grain size analysis chart of five samples. b) Particle size distribution graph showing positive-negative skewness comprising coarse-fine to silt-clay grains samples. c) Plasticity Chart plotted of each sample. d) Percentage of plasticity limits for each sample in the studied area.

Table 1. Percentage of Plasticity Limit for Each Sample in the Studied Area

Sampel	Particle size distribution			D10	D30	D60	Coefficient of uniformity, Cu, [D60/D10]	Coefficient of curvature, Cc, [(D30)²/ D60xD10]	Soil quality (USCS)
	Sand (%)	Silt (%)	Clay (%)						
L1-S1	7.71	82.46	9.83	2.04	8.23	20.02	9.81	1.66	Well
L1-S2	99.73	0.17	0.10	0.67	1.4	2.5	3.73	1.17	Well
L1-S3	48.65	27.71	23.64	0.052	0.06	0.11	3.6	0.63	Poor
L2-S1	9.81	83.57	6.63	2.86	9	25	8.74	1.13	Well
L2-S2	99.79	0.12	0.09	0.5	1.0	1.9	3.8	1.05	Well
L2-S3	35.06	31.14	33.80	0.05	0.08	0.18	3.6	0.71	Poor

plotted on a plasticity chart to identify the soil plasticity and organic properties in fine-grained soils for soil classification.

Liquid Limit

The liquid limit test results revealed that sample L1S3 exhibited the highest liquid limit percentage at 62 %, followed by sample L1S1 with 54 %. Samples L2S1 and L2S2 recorded the lowest liquid limit percentages at 36 % and 34 %, respectively (Table 2). The high percentage in sample L1S3 suggests it consists of residual granite soil, which according to Tan (2004), contains higher water content. This elevated liquid limit for residual granite soil can be attributed to particle size distribution. The liquid limit represents the water content at which soil transitions from a plastic to a liquid state. Soil with water content above the liquid limit may experience structural failure when it can not sustain stress under high moisture conditions (Jiang and Cui, 2022; Wang *et al*., 2024). Samples L1S2 and L2S1 showed lower liquid limits, possibly because they originate from residual metamorphic soil. Soils with lower liquid limit values have a reduced capacity to handle stress. There is a clear relationship between clay content and liquid limit, showing mutual dependence. Liquid limit values play a critical role in slope design as they help predict soil strength under stress. Considering Malaysia tropical climate and high annual rainfall, the liquid limit study assists engineers in designing stable slopes.

Plastic Limit

Plastic limit tests indicated that sample L1S3 had the highest percentage at 34 %, followed by sample L1S1 at 31 %, sample L2S2 at 26 %, sample L2S3 at 25 %, and samples L1S2 and L2S1 at 24 % and 20 %, respectively (Figure 4d). Table 2 details the plasticity index values for each sample type. Calculations show plasticity indexes ranging from 10 % to 28 %, with notably high plasticity indexes in samples L1S1, L1S3, and L2S2. Soil classification was based on data plotted on the plasticity chart. According to the Unified Soil Classification System (USCS), analysis indicated that samples L1S2 and L2S2 fell above the A-line, and were classified as clay. Meanwhile, samples L1S1, L1S3, and L2S1, falling below the A-line, were classified as silt. Samples L1S2, L2S2, and L2S3 were categorized as CI, indicating clay with moderate plasticity.

Table 2. Information on Liquid Limit, Plastic Limit, Plasticity Index, And Soil Classification for Each Sample

Sample	Liquid limit, LL (%)	Plastic limit, PL (%)	Plasticity index, PI (%)	Soil classification system (USCS, ASTM D2487)
L1S1	54	31	23	MH
L1S2	36	20	16	CI
L1S3	62	34	28	MH
L2S1	34	24	10	ML
L2S2	47	26	21	CI
L2S3	42	25	17	CI

Given their liquid limit below 50 % per ASTM D2487 classification, they are regarded as clayey silt. Samples L1S1 and L1S3 were classified as MH, referring to silt with high plasticity. Sample L2S1 was categorized as ML due to its liquid limit falling within the 34 % range, denoting a low plasticity index (Figure 4c). Soil failure occurs when it reaches its maximum stress level at a specific strain value. Plastic soil can endure an increase in strain within the soil. Soil failure due to peak stress may continue to bear stress, albeit with diminishing stress levels. According to Holtz and Kovacs (1981), soil that is semi-solid or brittle can withstand maximum applied stress, but will fail immediately afterward.

Riverbank Erosion

River bank erosion has been observed along the riverbank of the Belukar Bukit recreation centre (Locality 1). Erosion affects an area approximately 100 m horizontally, causing the banks, pedestrian infrastructure, trees, and built structures on the riverbanks to erode (Figures 5a and b). Furthermore, the erosion caused a small landslide scarp after the flood (Figure 5c). The height from the base to the surface of the eroded cliff reaches up to 3 m (Figure 5d). Additionally, the water has dredged up to 2 m towards the riverbank. Such severe erosion is likely to occur when the water flow is fast, and the water level surpasses the original riverbanks. This is evidenced by several uprooted trees, collapsed road and clay sediment in the riverbank toe due to affected by the water flow (Figure 6). According to Lemnitzer *et al*. (2023), the erosion mechanism of the riverbank results in wide scouring at the bottom of the steep bank, leading to landslides during high water levels. Another contributing factor is that the area of Belukar Bukit is closest to the water source, experiencing the highest pressure compared to downstream areas. Increased water velocity exerts stronger pressure on fine-sized soil types compared to river sediments such as pebbly rocks, making them more susceptible to erosion by water. Analysis of the eroded area reveals that the soil at the bottom of the cliff (i.e., L2S1) consists dominantly of silt (Table 1).

Mass Movement /Wasting

The phenomenon of mass movement/riverbank failure on the sandy cliffs/slopes occurs along the riverbanks in the Belukar Bukit Village area (Locality 2). Mass movement that occurs around this river (suspect to occur during the monsoon season of December to March) shows that the banks are unstable, and are easily eroded by water currents. This is because riverbanks always experience fluvial hydraulic erosion and geotechnical instability (*i.e.* gravitational instability) processes that will lead to bank failure (Surian and Rinaldi, 2003; Islam, 2008; Zhao *et al*., 2022; Zhou *et al*., 2024). This two process often linked together. Fluvial erosion is the scouring of materials from bank toe by flowing water once the hydraulic force of the river exceeded the resistance threshold of the bank material, thus increasing bank angle and reduce bank stability (Langendoen and Simon 2008; Langendoen *et al*., 2009). Sediment transport will be initiated when the shear stress overcomes bank material strength that causes the soil particles to be entrained. This happens because shear stress increases as flow increases, while bank material strength normally decreases as bank becomes saturated. This erosion leads to unstable bank, because the forces supporting the weight of the upper bank are reduced (Baracos and Lew, 2003; Lemnitzer *et al.*, 2023). Gravitational failures are frequently preceded by fluvial erosion, which is also responsible in transporting the debris created by gravitational failures. Bank sediments experience varying levels of shear stress due to differences in water pressure along the slope where sediment particles located at the bottom of the slope encounter higher hydraulic head and consequently, more stress than those located higher up the bank where the hydraulic head is lower (Staley *et al*., 2006; Zhao *et al*., 2022). This results in a gradient of shear stresses across the bank. The difference in shear stress also leads to the formation of a zone where the bank erodes at a faster rate, particularly at the bottom of the slope, which eventually creates steep or overhanging slopes.

The greatest erosion suggested occurred due to flowing water from the nearest dam (*i.e.* Sultan Mahmud Dam) occupy high energy will be con-

Figure 5. a) A house hanging near the riverbank due to erosion at locality 1. b) Road damage caused by water overflow during the flood at locality 1. c) A small scarp formed by a landslide on the steep riverbank after the flood at locality 1. d) Erosion occurring in the riverbank area at locality 1. e) and f) Tarred road fragments at the foot of the bank due to the riverbank collapse. g) An effect of erosion on the steep riverbank, eventually causing a landslide from a different angle. h) Vegetation fell due to a landslide on the riverbank, caused by erosion at Locality 1.

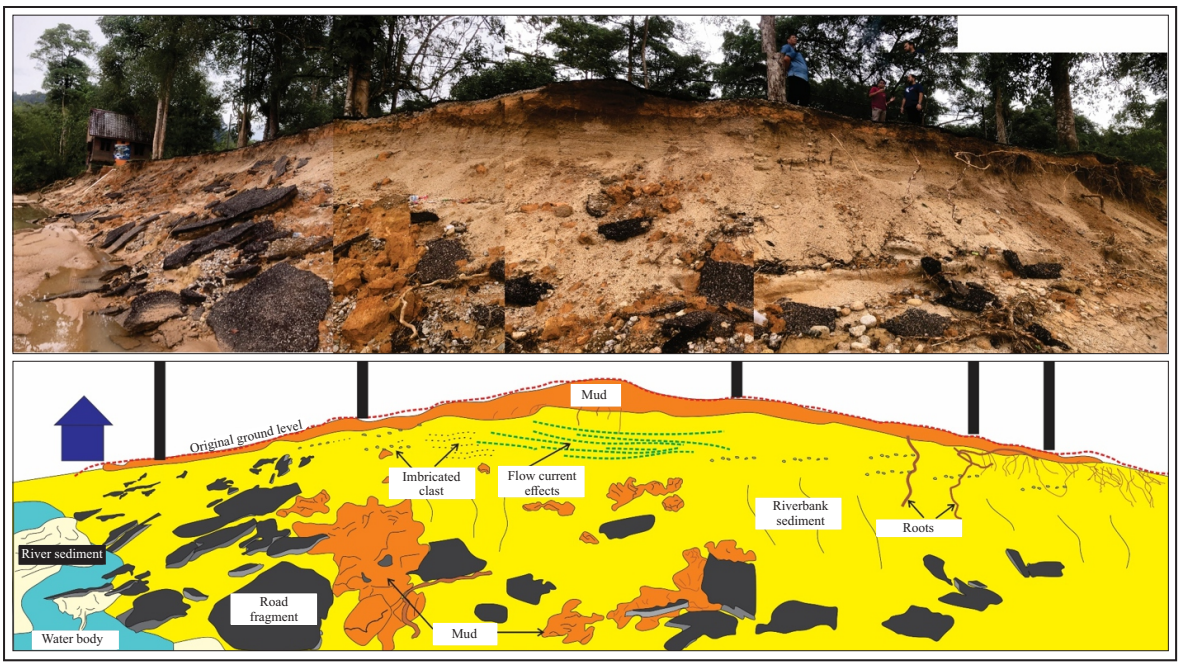

Figure 6. Anatomical sketch of erosion in the Belukar Bukit Waterfall area, Ajil after the rise in water level and also the rapid water current. Clearly observed the effect of waterways through the arrangement of imbrication of pebbles on the riverbanks. Clay sediment as well as broken roads can be seen in the lower part of the river.

sidered as a main factor for erosion. The erosion will take place on the lower part of riverbank by scouring and dreging the bank. The observation has been taken on the riverbank slide. The estimated distance of the landslide from field observations can reach more than 50 m horizontally (Figures 5e and g). The ruins of this riverside slope originally had a tarred road used by local residents. Now, fragments of the road and vegetation can still be seen on the lower riverbank (Figures 5f and h). The original distance between the riverbank and the shoulder of the road is 6 m, and when the collapse occurred, part of the road in the middle collapsed (Figure 7). The collapse of the slope occurs vertically, indicating that the slope is very steep.

Slope measurements (dips) were recorded in the studied area with relatively high slope values of 60° to 70° and a slope direction of 305°. Using the friction angle, Φ, of 31°, a simple kinematic model has been made using a stereonet to determine the type of failure (Figure 8). When a flood recedes, the planar type of riverbanks is usually affected by significant erosion due to several factors. These include; (1) the reduction of the hydrostatic

Figure 7. Sketched area of the broken road due to the occurrence of a landslide, also clearly observed the breakdown of the tar road at the bottom of the slope.

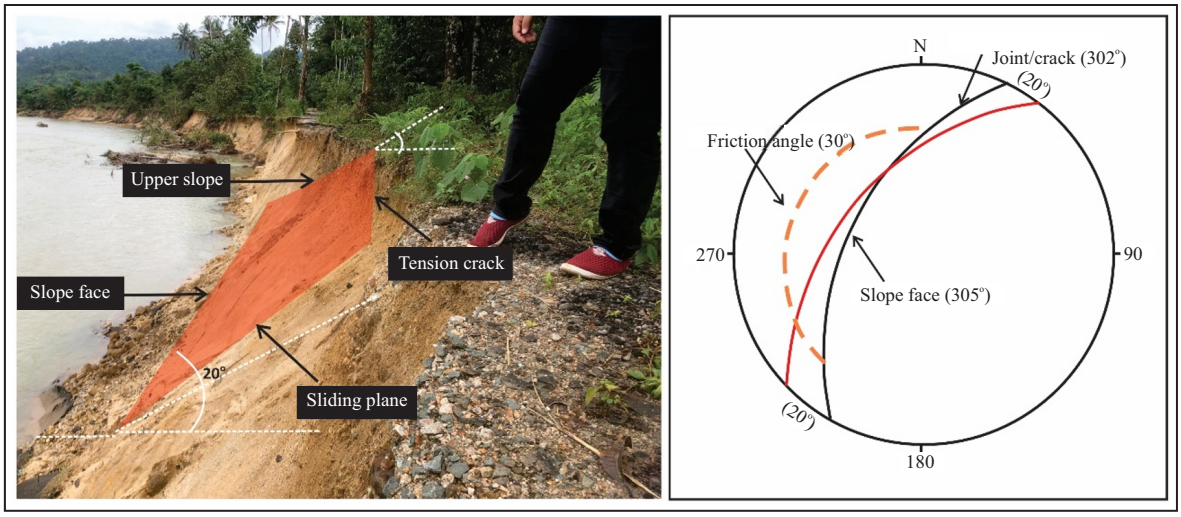

Figure 8. A field observation analysis of the steep river slope in Sungai Berang at locality 2. A geometric sketch was drawn for the purpose of making it easier to observe mass movement on the river slope. Next to the picture is a geometric sketch showing a kinematic model that is analyzed as a planar failure of the soil due to the sliding plane (friction angle) < the crack (sliding surface angle) < the slope face angle (slope face angle) and the crack plane is parallel to the slope face.

force/pressure caused by the decrease in the water level (Pasha *et al*., 2025; Eskandarinejad *et al*., 2025), (2) the time delay between the lowering of the water level in the river and the underground water level which generates a significant uplift force (Wang *et al*., 2020; Ren *et al*., 2022), and (3) the decrease in suction force and apparent cohesion caused by the infiltration of rainwater or groundwater seepage (Rinaldi and Casagli, 1999). When a slope is steep, the failure is likely to happen on a smooth and level surface where the block slides into the channel without any rotation.

Conclusions

Observations at the initial stage of the study found that some study localities have experienced river erosion and also quite severe landslides, especially in the area of Belukar Bukit Waterfall and river in the area of Belukar Bukit Village. In addition, the slope angle of the river bank plays a very important impact in the scouring/dredging process by the water current. The bigger the slope, the bigger the acting current, the more unstable the slope and the more soil loss. The riverbanks in Hulu Terengganu show significant erosion and mass movement, with layers of lithological units that reflect dynamic sedimentary processes driven by fluctuations in river flow, particularly during flood events. Riverbank 1 shows a sequence of cross-bedded gravel (Litho B), unsorted coarse grains (Litho C), and compacted sand-silt with oxidized plant roots (Litho D), indicating varying energy conditions. Riverbank 2, standing higher and showing more extensive erosion, features similar layers but with thicker cross-bedding and a more prominent erosional base, suggesting stronger flood influences. Physical test analysis reveals a predominance of sand with variations in silt and clay, affecting soil stability, with well-graded soils contributing to stability and poorly graded soils indicating potential compaction issues. Severe erosion and mass movements, especially during the monsoon, have significantly impacted the riverbanks, leading to infrastructure damage and highlighting the area vulnerability to further landslides and erosion due to the steep slopes, hydraulic forces, and soil characteristics.

Acknowledgments

This research was funded by the Terengganu Strategic and Integrity Institute (TSIS) research grants. The authors also thank Mohamad Hakim

Mohd Shukri, A'li Naufal Allias, Muhammad Thareq A. Aziz, Muhammad Fauzi Rodzee, and Muhammad Hafiz Jamaludin for their assistance in the field.

References

Ahmed, I., 2001. Rivers and Environmental Refugees. *Indian Journal of Landscape Systems and Ecological Studies,* 24, p.120-130.

Badruldin, M.H., Ghani, A.A., and Quek, L.X., 2017. Petrogenesis of Ajil mafic dykes from Eastern Belt of Peninsular Malaysia: fractionated within plate lithospheric mantle magma beneath the eastern Malaya Block. *Current Science,* 113 (7), p.1448-1455. DOI: 10.18520/cs/v113/i07/1448-1455.

Baracos, A. and Lew, K.V., 2003. *Riverbank Slides, Erosion and Deposition at 758 Crescent Drive, Winnipeg, Manitoba - Volume 1 Report*. Retrieved from Department of Justice Canada, Winnipeg, Manitoba.

Casagrande, A., 1948. Classification and Identification of Soils. *Transactions*, *ASCE,* 113, p.901-930.

Casnedi, R. and Giulio, A.D., 1999. Sedimentology of the Section Peak Formation (Jurassic), Northern Victoria Land, Antarctica. *Special Publications of the International Association of Sedimentologists*, 28, p.435-448. DOI:10.1002/9781444304213.ch30.

Chassiot, L., Lajeunesse, P., and Bernier, J.F., 2020. Riverbank erosion in cold environments: Review and outlook. *In*: *Earth-Science Reviews,* 207, 103231. DOI:10.1016/j.earscirev.2020.103231.

Darby, S.E. and Thorne, C.R., 1996. Numerical simulation of widening and bed deformation of straight sand bed channels. *In*: *Model development, Journal of Hydraulic Engineering. ASCE,* 122 (4), p.184-193. DOI:10.1061/(ASCE)0733-9429(1996) 122:4(184).

Das, B.M. and Sobhan, K., 2018 *Principles of geotechnical engineering. 9th ed*. Boston, MA: Cengage Learning.

Duan, H., Zou, L., and Cvetkovic, V., 2024. Sensitivity analysis of hydraulic erosion and calibration of the erosion coefficient. *Engineering Geology*, 338, 107624.

Duró, G., Crosato, A., Kleinhans, M.G., Roelvink, D., and Uijttewaal, W.S.J., 2020. Bank Erosion Processes in Regulated Navigable Rivers. *Journal of Geophysical Research: Earth Surface*, 125 (7), p1-26. DOI:10.1029/2019JF005441.

Eskandarinejad, A., Nazari, R., Nikoo, M.R., Arellano, D., Pezeshk, S., and Ghasemi, S.H., 2025. A comprehensive review of geotechnical implications of floods and water-driven disasters. *Science of the Total Environment*, 985, 79731.

Gasim, M.B., Othman, M.S., and Chek, T.C., 2005a. Total flows contribution of the Tasik Chini feeder rivers and its significant water level, Pahang, Malaysia. *Proceedings of the 6th ITB-UKM Joint Seminar on Chemistry*. Sanur Paradise Plaza Hotel, Bali, Indonesia, 16-20 May 2005. p.543-547. Retrieved from https://repository.bbg.ac.id/bitstream/339/1/JSChem_ITB-UKM_VI-2005.pdf.

Hao, Y., Jia, D., Zhang, X., Shang, Q., Zhu, H., Fei, X., Yang, J., Wu, L., and Chen, C., 2023. Stability analysis of riverbanks with a dual structure under water-root-soil coupling. *Water Science and Technology*, 88 (3), p.658-676.

Holtz, R.D. and Kovacs, W.D., 1981. *An Introduction to Geotechnical Engineering.* Eaglewood Cliff, NJ: Prentice-Hall, Inc. 733pp.

Huang, D., Huang, W.B., Ke, C.Y., and Song, Y.X., 2021. Experimental investigation on seepage erosion of the soil-rock interface. *Bulletin of Engineering Geology and the Environment.* 80, p.3115-3137.

Islam, M.S., 2008. Riverbank Erosion and Sustainable Protection Strategies. Fourth International Conference on Scour and Erosion. Retrieved from https://www2.kuet.ac.bd/JES/images/files/v2/02_08.pdf.

Jiang J.J. and Cui, Z.D., 2022. Instability of high liquid limit soil slope for the expressway induced by rainfall. *Applied Sciences,* 12 (21),10857. DOI: 10.3390/app122110857.

Julian, J.P. and Torres, R., 2006. Hydraulic erosion of cohesive riverbanks. *Geomorphology*, 76 (1-2). DOI:10.1016/j.geomorph.2005.11.003.

Langendoen, E.J. and Simon, A., 2008. Modeling the Evolution of Incised Streams. II: Streambank Erosion. *Journal of Hydraulic Engineering,* 134 (7), p.905-915. DOI:10.1061/(ASCE)0733-9429(2008)134:7(905).

Langendoen, E., Lowrance, R., and Simon, A., 2009. Assessing the impact of riparian processes on streambank stability. *Ecohydrology, 2*, p.360-369. DOI:10.1002/eco.78.

Lemnitzer, A., Gardner, M., Stark, N., Nichols, E., George, M., Müller, J., Stamm, J., Zimmermann, R., Schüttrumpf, H., Wolf, S., Burghardt, L., and Klopries, E., 2023. Geotechnical and geo-environmental damage and its impacts on critical community infrastructure during the 2021 Western European floods: the case study of Altenahr, Germany. *9th International Congress on Environmental Geotechnics. Chania*, p.474-488. DOI:10.53243/ICEG2023-428.

Pasha, G.A., Asghar, M., Murtaza, N.,and Ghumman, A., 2025. Impact of floating debris on houses during floods and vegetation-based mitigation. *Proceedings of the Institution of Civil Engineers. Water management,* 178 (2), p.126-141.

Rahman, M.N.I.A., Roslan, A.N., Wali, S.S.A.S., Baharim, N.B., Ghani, A.A., and Ali, C.A., 2023. Petrographic Features and Modelling of Some Waterfall Rocks in Kenyir Lake, Terengganu: A Microscopic Perspective Approach in Sustainable Geotourism. *Journal of Sustainability Science and Management*, 18 (2), p.51-66. DOI:10.46754/Jssm.2032.02.005.

Razali, I.H., Mohd Taib, A., Ab. Rahman, N., Abang Hasbollah, D.Z., Md. Dan, M.F., Ramli, A.B., and Ibrahim, A., 2023. Slope stability analysis of riverbank in Malaysia with the effects of vegetation. *Physics and Chemistry of the Earth*, 129. DOI:10.1016/j.pce.2022.103334.

Ren, Z., Lu, Q., Liu, K., Ni, P., and Mei, G., 2022. Model-scale tests to examine water pressures acting on potentially buoyant underground structures in clay strata. *Journal of Rock Mechanics and Geotechnical Engineering*, 14 (3), p.861-872. DOI:10.1016/j.jrmge.2021.09.014.

Rinaldi, M. and Casagli, N., 1999. Stability of streambanks formed in partially saturated soils and effects of negative pore water pressures: The Sieve River (Italy). *Geomorphology,* 26 (4), p.253-277.

Saikia, S. and Laskar, J.J., 2022. Fine Grained Braided River Sedimentation in Brahmaputra River, Majuli, Assam, India. *Journal of the Geological Society of India*, 98 (10), p???-???. DOI:10.1007/s12594-022-2189-5.

Sharoum, F.M., Abdullah, M.T., Ali, C.A., and Ismail, R., 2015. *Geopark Tasik Kenyir*. Universiti Malaysia Terengganu, 104pp.

Staley, N.A., Wynn, T., Benham, B., Yagow, G., and Tech, V., 2006. Modeling channel erosion at the watershed scale: Model review and case study. Center for TMDL Watershed Studies, *Biological Systems Engineering, Virginia Tech. Document* (2006-0009).

Surian, N. and Rinaldi, M., 2003. Morphological response to river engineering and management in alluvial channels in Italy. *Geomorphology,* 50 (4), p.307-326.

Taha, N.A., Shariff, M.S.M., and Ladin, M.A., 2022. Case Study on Analyses of Slope Riverbank Failure. *Modelling and Simulation in Engineering*, *2022*. DOI:10.1155/2022/1965224.

Tan, B.K., 2004. *Country case study: engineering geology of tropical residual soils in* Malaysia.

Toriman, M.E., 1997. The effect of urbanization on riverbank erosion and lateral channel change of the Chorlton Brook, Manchester. *Jurnal Ilmu Alam.* 23, p.115-132.

Toriman, M.E., 2005. Hydrometeorological conditions and sediment yield in the upstream reach of Sungai Bebar, Pekan Forest Reserve, Pahang. *Biodiversity expedition Sungai Bebar Pekan Pahang. PSF Technical Series No.4.* UNDP/GEF Funded. Forest Research Institute Malaysia. p.41-45.

Toriman, M.E. and Che' Lah, H., 2007. Ciri Hidrologi Dan Hakisan Tebing Sungai di Sungai Lendu, Alor Gajah, Melaka. *Journal of E-Bangi,* 2 (2), 12pp. Retrieved from https://journalarticle.ukm.my/1545/1/ekhwan07.pdf.

Wang, D.D., Song, X.J., Wang, L.X., and Xu, H.B., 2024. Mechanical properties of structured high liquid limit clay under maximum drying stress conditions. *Geomatics, Natural Hazards and Risk,* 15 (1), 2324971, DOI: 10.1080/19475705.2024.2324971.

White, R.E., 2006. *Principles and Practice of Soil Science the Soil as a Natural Resource*. 4th ed. Blackwell Science Ltd. 386.

Zhao, K., Coco, G., Gong, Z., Darby, S.E., Lanzoni, S., Xu, F., 2022. A review on bank retreat: mechanisms, observations, and modeling. *Reviews on Geophysics,* 60, e2021RG000761.

Zhou, Y., Xia, J., Deng, S., and Han, Z., 2024. Bank erosion under the impacts of hydraulic erosion, river stage change and revetment protection in the Middle Yangtze River. *Geomorphology*, 448. DOI:10.1016/j.geomorph.2023.109043.